Electrorheological fluids: structures and mechanisms

Weijia Wen, Xianxiang Huang and Ping Sheng*

Received 17th July 2007, Accepted 26th September 2007
First published as an Advance Article on the web 23rd October 2007
DOI: 10.1039/b710948m

Electrorheology denotes the control of a colloid's flow properties through an electric field. We delineate the basic characteristics of electrorheological (ER) fluids, and show that the use of an effective dielectric constant concept can yield quantitative predictions. In particular, the ground state structure, the structural transition that occurs under crossed electric and magnetic fields, the high-field yield stress and its variation with particle size are all in good agreement with the experiments. The recently discovered giant electrorheological effect, owing its origin to molecular dipoles, is described and contrasted with the conventional ER effect that arises from induced polarization effects.

1. Introduction

Electrorheological fluids are a type of "smart" colloid capable of varying viscosity or even solidification in response to an applied electric field. The rheological variation is reversible when the field is removed. The response time can be as short as a few milliseconds. Due to such marvellous features, ER fluids can serve as an electric–mechanical interface, and when coupled with sensors to trigger the electric field, can turn many devices such as clutches, valves, dampers *etc*. into active mechanical elements capable of responding to environmental variations—hence the denotation "smart" fluid. The diverse applications potential[1–7] has made ER fluids a persistent area of study in soft matter research, ever since their discovery six decades ago. However, in spite of the broad interest, applications have been hampered by the weakness of the ER effect. This state of affairs was changed in recent years owing to the discovery of the giant electrorheological (GER) effect,[8,9] which represents a different paradigm from the conventional ER mechanism. The discovery of the GER effect also facilitated the application of ER fluids in various devices.

Department of Physics and the Institute of Nano Science and Technology, The Hong Kong University of Science and Technology, Clear Water Bay, Kowloon, Hong Kong. E-mail: sheng@ust.hk; Fax: (852) 2358 1652; Tel: (852) 2358 7506

In what follows, a brief review of the conventional ER mechanism and the conceptual advance that made its quantitative modeling possible are given in Section 2. Comparison with experiments, in particular the ground state structure(s), the yield stress, the upper bound and its variation with particle size, and the nonlinear and anisotropy of the effective dielectric constant, are detailed in Section 3 together with an explanation of the physical underpinnings. The motivation and discovery of the GER effect are presented in Section 4, together with a phenomenological theory of its mechanism.

2. The electrorheological (ER) effect and its mechanism

The electrorheological effect was discovered some sixty years ago, widely credited to Winslow.[10] It remained as a curiosity until the 1980's, when renewed experimental and theoretical interests advanced both our understanding of the ER mechanism(s) as well as the fabrication of novel materials with enhanced ER effect.[11]

2.1 Heuristic theory

A heuristic description of the ER effect is as follows. Owing to the dielectric constant contrast between the solid particles and

Weijia Wen

Weijia Wen's main research interests include soft condensed matter physics, electrorheological (ER) and magnetorheological (MR) fluids, field-induced pattern and structure transitions, micro- and nano-fluidic control, microsphere and nanoparticle fabrication, thin film physics, band gap materials, metamaterials and nonlinear optical materials.

Ping Sheng

Ping Sheng is the Dr William Mong Chair Professor of Nanoscience at the Hong Kong University of Science and Technology, and Head of the physics department. His research interests are in complex fluids, hydrodynamic boundary conditions, electrorheological fluids, photonic and phononic wavefunction materials, and carbon nanotube superconductivity.

the liquid in a colloid, each solid particle would be polarized under an electrostatic field, with an effective dipole moment. The resulting (induced) dipole–dipole interaction means that the particles tend to aggregate and form columns along the applied field direction. The formation of columns is the reason why the high-field state of an ER fluid exhibits increased viscosity or even solid-like behavior, able to sustain shear in the direction perpendicular to the applied electric field.[12–20] This picture is schematically illustrated in Fig. 1.

However, such a simple heuristic picture leaves many questions unanswered. In particular, as the particles aggregate and touch, multipole interactions (those beyond the dipole interaction) necessarily become dominant, and local field effects must also be taken into account. The conductivity and/or relaxational effects, appearing as the imaginary part of the particle and/or fluid dielectric constants, may also contribute to the ER effect. These complications make direct simulation of the ER effect quite difficult, and their characteristics beyond accurate theoretical prediction. In particular, for applications it is desirable to have an upper bound on the ER effect, so that devices may be designed accordingly.

2.2 Effective dielectric constant formulation

The conceptual advance that made the quantitative modeling of the ER effect possible is the formulation and description of the ER characteristics, consisting of the ground state microstructure of the solid microparticles under a high electric field and its relevant stress–strain relation, in terms of the effective dielectric constant variation. Upper bounds on the high-field shear modulus and yield stress may also be derived. In this formulation, the starting point is the observation that the static (or low frequency) electrical response of any composite material is characterized in general by an effective dielectric tensor $\tilde{\varepsilon}_{\text{eff}}$:

$$\boldsymbol{D} = \tilde{\varepsilon}_{\text{eff}} \boldsymbol{E} \tag{1a}$$

where

$$\tilde{\varepsilon}_{\text{eff}} = \begin{pmatrix} \bar{\varepsilon}_{xx} & \bar{\varepsilon}_{xy} & \bar{\varepsilon}_{xz} \\ \bar{\varepsilon}_{yx} & \bar{\varepsilon}_{yy} & \bar{\varepsilon}_{yz} \\ \bar{\varepsilon}_{zx} & \bar{\varepsilon}_{zy} & \bar{\varepsilon}_{zz} \end{pmatrix} \tag{1b}$$

Here $\boldsymbol{D}$ denotes the displacement field, $\boldsymbol{E}$ the electric field, and the matrix elements of $\tilde{\varepsilon}_{\text{eff}}$ are complex in general, with the imaginary part attributable to either DC electrical conductivity or dielectric relaxation. The effective dielectric constant concept is based on the nature of electromagnetic wave interaction with inhomogeneous materials. When the frequency of the electromagnetic wave is sufficiently low that its relevant wavelength is much larger than the scale of the inhomogeneities, microstructure can no longer be resolved and the composite appears homogeneous to the probing wave. In that limit the electromagnetic response is fully captured by the effective dielectric constant tensor, which would simplify to an effective dielectric constant when the material is isotropic.

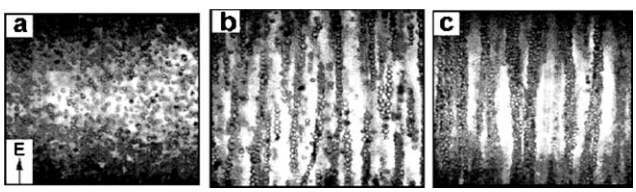

Fig. 1 The structural evolution of dielectric microspheres under an increasing electric field, from (a) no field, to (b) a moderate field of 500 V mm^{-1}, to (c) a strong field of 900 V mm^{-1}. Here the ER fluid consists of 1.5 micron glass spheres suspended in silicone oil.

It is important to note that the magnitudes of the effective dielectric constant tensor's matrix elements do depend on the relative volume fraction(s) of the constituents, as well as the anisotropy and the microstructure. This aspect is important in our considerations below.

The effective dielectric constant formulation treats the ER fluid as a fluid–solid composite in which the fluid is the matrix component. At the operating frequencies of the applied electric field (generally less than 10 kHz), electrical response can be characterized as being in the long wavelength limit. Hence the electrostatic Gibbs free energy density f of the system is given by

$$f = \frac{1}{8\pi} \boldsymbol{E} \cdot \text{Re}(\tilde{\varepsilon}_{\text{eff}}) \cdot \boldsymbol{E} - TS = -\frac{1}{8\pi} \text{Re}(\bar{\varepsilon}_{zz}) E^2 - TS \tag{2}$$

where the electric field is assumed to be applied along the z direction, Re( ) means taking the real part of the quantity in the parentheses, T denotes temperature, and S the entropy of the system. Since in most cases the electrical part of the free energy is much larger than the entropy part, the second term on the right hand side of eqn (2) is usually ignored. Through eqn (2), the ground state microstructure for an ER fluid with equal-sized solid microspheres may be obtained by maximizing the real part of the zz component of the effective dielectric constant tensor, with respect to the positions, *i.e.*, the microstructure, of the microspheres. Here the (valid) assumption is that the ground state must have a periodic structure, since it is unique. The shear modulus and the yield stress may be obtained from the ground state microstructure by defining the local shear distortion, and calculating the free energy difference from the ground state. The yield stress, if there is one, is defined to be the maximum point of the shear stress *vs.* shear strain plot, beyond which the shear stress decreases with increasing strain, implying instability.

The advantage of this approach is that it solves, in one step, all the difficulties posed earlier. In particular, the local field effect and the multipole interactions are all accounted for, provided the effective dielectric constant can be accurately evaluated. In addition, the contribution of the imaginary part of the dielectric constant may also be incorporated, as seen below.

2.3 Bergman–Milton spectral representation

Since the essence of calculating the free energy lies in the evaluation of the effective dielectric constant, a rigorous approach to $\tilde{\varepsilon}_{\text{eff}}$ is desirable. This is because we want to distinguish the energies of different microstructures for the (equal-sized) microspheres, *e.g.*, body centered tetragonal (BCT) structure *versus* the face centered cubic (FCC) structure. And these differences can be quite small and would not show up in the usual

effective medium theories. In fact, the small differences between the different microstructures are manifest only at high filling fractions of the microspheres, since in that limit there can be differences in the local environment for the different periodic structures. The Bergman–Milton spectral function representation of the effective dielectric constant[21–24] provides the perfect approach to distinguish the structures from the value of $\bar{\varepsilon}_{zz}$. The starting point of its derivation is the Laplace equation

$$\nabla\cdot[\varepsilon(\boldsymbol{r})\nabla\phi(\boldsymbol{r})]=0 \tag{3}$$

Here ϕ is the electrical potential, *i.e.*, $\boldsymbol{E}=-\nabla\phi$, and $\varepsilon(\boldsymbol{r})$ is the local dielectric constant, given by

$$\varepsilon(\boldsymbol{r})=\varepsilon_{\mathrm{l}}\left[1-\frac{1}{s}\eta(\boldsymbol{r})\right] \tag{4}$$

where

$$s=\frac{\varepsilon_{\mathrm{l}}}{\varepsilon_{\mathrm{l}}-\varepsilon_{\mathrm{s}}} \tag{5}$$

ε_{l} being the liquid dielectric constant and ε_{s} the solid dielectric constant. Here η is the characteristic function, defined to be 1 inside the solid particles, and zero elsewhere. The characteristic function contains all the geometric information of the problem. By rewriting eqn (5) as

$$\nabla^2\phi(\boldsymbol{r})=\frac{1}{s}\nabla\cdot[\eta(\boldsymbol{r})\nabla\phi(\boldsymbol{r})] \tag{6}$$

with the boundary conditions $\phi(x, y, z = 0) = 0$ and $\phi(x, y, z = L) = L$ (*i.e.*, average $E_z = -1$), the potential ϕ may be formally solved as

$$\phi=z+\frac{1}{s}\hat{\Gamma}\phi \tag{7a}$$

or

$$\phi=\left(1-\frac{1}{s}\hat{\Gamma}\right)^{-1}z \tag{7b}$$

where $\hat{\Gamma}$ is an integral operator defined by

$$\hat{\Gamma}\phi(\boldsymbol{r})=\int dV'\eta(\boldsymbol{r}')\nabla'G(\boldsymbol{r},\boldsymbol{r}')\cdot\nabla'\phi(\boldsymbol{r}') \tag{8}$$

and $G(\boldsymbol{r},\boldsymbol{r}')=1/4\pi|\boldsymbol{r}-\boldsymbol{r}'|$ is the Green function of the Laplacian. The integral operator $\hat{\Gamma}$ is Hermitian under the following definition of the inner product:

$$\langle\psi|\phi\rangle=\int dV\eta(\boldsymbol{r})\nabla\psi^*(\boldsymbol{r})\cdot\nabla\phi(\boldsymbol{r}) \tag{9}$$

If ϕ_u and s_u are respectively the eigenfunctions and their associated eigenvalues of the integral (Hermitian) operator $\hat{\Gamma}$, then it is straightforward to express the zz component of the effective dielectric tensor in the *spectral representation* as

$$\bar{\varepsilon}_{zz}=\varepsilon_{\mathrm{l}}\left(1-\frac{1}{V}\sum_u\frac{|\langle z|\phi_u\rangle|^2}{s-s_u}\right) \tag{10}$$

where $\bar{\varepsilon}_{zz}$ is defined as the volume-averaged value of D_z divided by the volume-averaged value of the electric field, given simply by $E_z = -1$. In eqn (10), V, the sample volume, is a normalization factor. The most remarkable feature of eqn (10), which is exact, is the fact that material properties, given by s, are completely separated from the geometric information (contained in ϕ_u and s_u) as "filtered" by the Laplacian. Since both the solid and liquid dielectric constants can be complex, s is a complex number in general. At the same time, it is clear that if s is real, then its value as given by eqn (5) should be either less than zero or greater than 1. Since both $|\langle z|\phi_u\rangle|^2$ and s_u are real, with the additional (proven) constraint that $0 < s_u < 1$, it follows that $s - s_u$ can approach zero only in limiting cases, and these cases define the upper bounds for the shear modulus and yield stress, described below.

Eqn (10) makes it clear that the imaginary parts of the dielectric constants can indeed contribute to $\mathrm{Re}(\bar{\varepsilon}_{zz})$ (through the complex material parameter s), and hence the ER effect.

3. Modeling and comparison with experiments

Extensive amounts of theory and experiments have been carried out to clarify the ER mechanisms.[25–30] By using the spectral representation and the effective dielectric constant formulation, quantitative predictions became possible for the microstructure, shear modulus, yield stress, and other related characteristics associated with an ER fluid comprising uniform-sized microspheres. In particular, upper bounds can be derived for the shear modulus and yield stress. Details of the calculational approach can be found in ref. 24.

3.1 Ground state microstructure

For uniform-sized microspheres, the lowest energy state should correspond with a periodic microstructure which maximizes the overall effective dielectric constant of the system. By calculating the effective dielectric constants for the six structures of body centered tetragonal (BCT), face centered cubic (FCC), hexagonal close-packed (HCP), body centered cubic (BCC), simple cubic (SC), and diamond structures it was found that at any fixed concentration of solid microspheres, the magnitude of the effective dielectric constant always arranged themselves in the above decreasing order, with FCC and HCP a very close second to BCT. The calculated values of $\bar{\varepsilon}_{zz}$ for the various structures are shown in Table 1, at two ratios of $\varepsilon_{\mathrm{s}}/\varepsilon_{\mathrm{l}} = 10$ and 800. For comparison, calculations using just the dipole approximation are also shown.

In Table 1, it should be noted that the values of the effective dielectric constants given are those averaged over the whole sample. That is, for the effective dielectric constant values inside the close-packed columns, the FCC value is in fact larger

Table 1 The exact effective dielectric constants of several periodic structures, compared with that in the dipolar approximation. The separation between the spheres is 5×10^{-3} in terms of the sphere radius, and the volume fraction of particles is 0.2

		Structure					
$\varepsilon_{\mathrm{s}}/\varepsilon_{\mathrm{l}}$		BCT	FCC	HCP	BCC	SC	Diamond
10	Exact	2.167	2.156	2.156	2.043	1.911	1.627
	Dipole	2.031	1.994	1.995	1.905	1.734	1.601
800	Exact	5.173	5.129	5.129	4.205	3.518	1.976
	Dipole	3.376	3.188	3.194	2.798	2.230	1.897

than that for the BCT, owing to the higher packing density. However, when averaged over the whole sample, which can be done easily (by volume averaging the fluid dielectric constant and the column dielectric constant) owing to the columnar mesostructure, the BCT wins slightly. For the same reason that the BCT's value is lower in the columns (lower density than the FCC), it thereby has a higher volume fraction of the columns for a fixed overall volume fraction of solid particles (fixed at 0.2 for the results shown in Table 1). It turns out that BCT always wins slightly, regardless of the values of the material constants and solid volume fractions. However, being a very close second, FCC can win over BCT in a different situation, leading to a Martensitic transition. This is shown below.

Thus BCT is the ground state microstructure for the microspheres inside the solid columns formed under an external electric field.[19,31] This prediction remains unchanged for any ratio of the solid and liquid dielectric constants, and also remains true if the electrostatic interaction between the solid microspheres is treated only within the dipole approximation.[25]

Another interesting prediction is that if the microspheres are not only responsive to an electric field, but also responsive to a magnetic field (*e.g.*, by using a Ni coating so that each microsphere can have a small magnetic moment), then under crossed electric and magnetic fields there can be a structural Martensitic transition in the ground state structure, from BCT to FCC.[31] Physically this is based on the minimization of the electrostatic energy plus the magnetic energy. As the magnetic field increases and the magnetic energy becomes comparable to the electric energy, the ground state structure inevitably would tend towards a more symmetric structure along the two directions of the electric and magnetic fields, hence the FCC structure.

Experimentally, microspheres with a glassy core of 34 $\pm$ 2 μm were multiply-coated by a 2 μm layer of Ni, a 1.5 μm layer of lead zirconate titanate (PZT), another 1 μm layer of Ni, and finally a 1 μm layer of TiO_2. The overall diameter of the microspheres is thus 45 $\pm$ 2 μm. Cross-sectional SEM pictures of the coated spheres are shown in Fig. 2(a). The apparent size variation is caused by deviation of the spheres' centers from the cutting plane. A more detailed picture of the coatings is shown in Fig. 2(b). The magnetic response of these multiply-coated microspheres is demonstrated in Fig. 2(c), in which the microspheres are shown to stagger upright under the influence of a small magnetic stirrer.

We first investigate the ground state microstructure under an electric field of $E = 2$ kV mm^{-1} when the microspheres were dispersed in epoxy. After solidifying the epoxy matrix, the sample was cut along the (001) and (110) planes and visualized with SEM pictures. They are shown in Fig. 3(a) and 3(b), respectively. Together they uniquely determine the structure to be BCT.

A separate sample with similar composition was subsequently prepared and subjected to the same electric field but a varying magnetic field. The structural transition was monitored by measuring the small dielectric constant variation in the direction perpendicular to both the electric and magnetic fields. A clear minimum in the dielectric constant was observed in every case, between 50 G to 80 G. When the magnetic field is

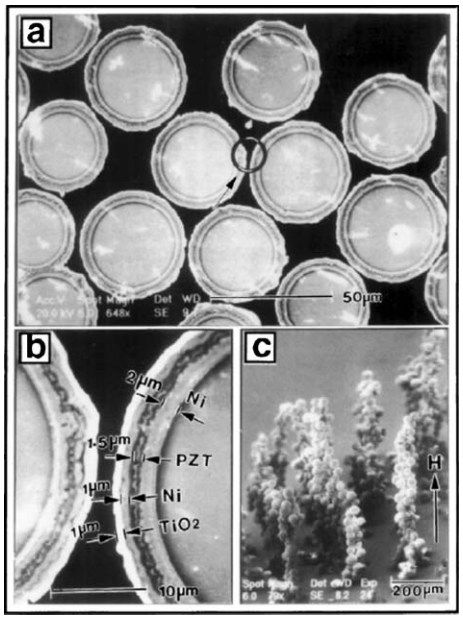

Fig. 2 (a) Cross-sectional SEM picture of the coated spheres. The apparent size variation is caused by deviation of the spheres' centers from the cutting plane. The arrow points to a circular region detailed in (b), which shows in detail the thickness of the four coatings. From the inside out: 2 μm Ni, 1.5 μm PZT, 1 μm Ni, and finally 1 μm TiO_2. (c) The coated EMR spheres under the influence of a small magnetic stirrer.

larger than that, the dielectric constant returns to that observed at the low field limit, indicating that the BCT structure is now established along the magnetic field direction instead of the electric field direction. However, in the interesting region of the minimum, we had obtained many cross-sectional micrographs by freezing in solid epoxy the

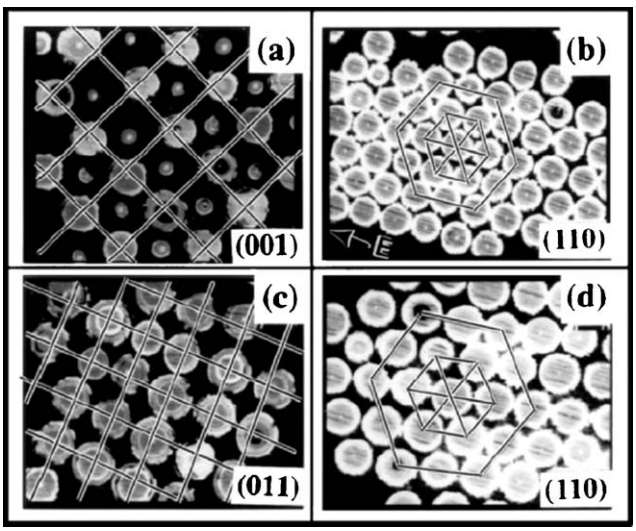

Fig. 3 (a) and (b) BCT structure formed by multiply-coated microspheres under an electric field (2 kV mm^{-1}). The structure is frozen in epoxy and visualized through cross-sectional SEM micrographs. (c) and (d) are the signatures of a FCC structure formed by the same multiply-coated microspheres under a crossed electric field (2 kV mm^{-1}) and magnetic field (54 G).

configurations at various magnetic field values, and cutting the resulting samples. The results are shown in Fig. 3(c) and 3(d). They indicate a square lattice in the (011) plane (the FCC {100}) and a hexagonal lattice in the (110) plane (the FCC {111}), both the signatures of a FCC structure.

The direct observation of the ground state microstructure and its Martensitic transition under crossed electric and magnetic fields clearly demonstrates the appearance of self-organized microstructures under external field(s), as predicted from energy considerations.

3.2 Shear modulus and yield stress

From the known ground state microstructure, one can calculate the shear modulus and yield stress by first defining the shear distortion. This is shown in the inset to Fig. 4. Here θ, the angle of distortion relative to the external field E, is the strain variable. For the BCT lattice, shearing in the direction perpendicular to the z axis means not only a tilt away from the electric field direction by an angle θ, but also a distortion in the lattice constants c and a given by $c/R = 2/\cos\theta$, $a/R = [8 - (c^2/2R^2)]^{1/2}$. Consequently, under shear the volume fraction of solid spheres in BCT structure is also θ dependent. For small θ, $\bar{\varepsilon}_{zz}(\theta)$ may be expanded about its optimal value as

$$\mathrm{Re}\left[\frac{\bar{\varepsilon}_{zz}(\theta)}{\varepsilon_1}\right] = \mathrm{Re}\left[\frac{\bar{\varepsilon}_{zz}(0)}{\varepsilon_1}\right] - \frac{1}{2}\mu\theta^2 + - - - \qquad (11)$$

where μ denotes the shear modulus. For finite distortions, the effective dielectric constant can again be calculated using the spectral representation, leading to an energy as a function of θ, $E(\theta)$. By definition the stress is given by $dE(\theta)/d\theta$. A numerically evaluated stress *versus* strain curve is shown in Fig. 4. It is seen that at small strain, the stress varies linearly with strain. And the slope of the linear variation is precisely the shear modulus. Also, the peak of the stress–strain curve corresponds to the yield stress (at the position of maximum strain) beyond which the system becomes unstable.

To experimentally verify the yield stress prediction, we utilize the relaxational effect of the dielectric constant that would generally appear at finite frequencies (of the applied electric field). It has been widely known in the field of ER fluid research that the presence of any water in the sample can enhance the ER effect, sometimes dramatically. And water is known to have a relaxational dielectric constant that can be strongly frequency dependent. In addition, water has a fairly large real part of the dielectric constant, and it was suspected that the early detected ER effect was due to the presence of water. But water can disappear starting at temperatures >60 °C, and hence can cause unreliable performance. The ER fluids produced after the 1980's have been especially noted to avoid any presence of water,[32–34] *e.g.*, in our experiments on visualizing the ground state microstructures, all samples were heated to 120 °C for 24 h prior to measurements. However, the role of water has always been intriguing, and a systematic study of the role of water would not only be informative in relation to the theory predictions, but also may be enlightening in the search for a type of colloids with enhanced ER effect.

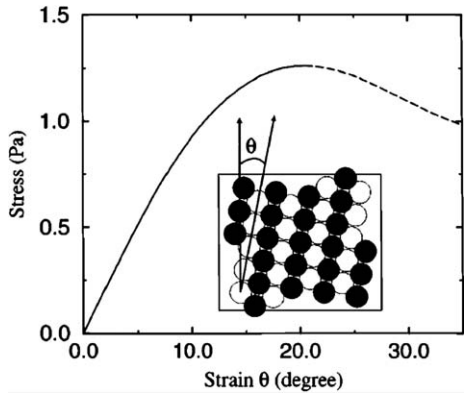

Fig. 4 Calculated stress, in units of Pascals, plotted as a function of strain, *i.e.*, the tilt angle θ as defined in the inset. The dashed line indicates the unstable regime. The maximum stress is defined as the static yield stress. Here the curve is calculated with $\varepsilon_l = 2.7$, $\varepsilon_s = 8.4 + 0.43i$, the volume fraction of spheres is 22%, and the applied field is 1.3 kV mm^{-1}.

Three samples were prepared, consisting of 1.5 μm diameter microspheres dispersed in silicone oil. The samples were first baked to remove any trace water, and then a measured amount of 5 vol% (denoted sample 1), 8 vol% (sample 2), and 11.4 vol% (sample 3) water were introduced.[35] With a cell comprised of two parallel plate electrodes, the dielectric measurements of the ER fluids were performed by an HP4284A LCR meter in a frequency range of 20 Hz to 100 kHz. The static yield stress was measured by using a standard parallel plate torsional device with a root-mean-square (RMS) electric field of 510 V mm^{-1} applied across the ER fluids sandwiched between the two parallel plates. The lower plate was rotated slowly, dragging the top plate with a torque, which was connected *via* a torque meter to the top plate. The static yield stress was read out when slipping occurred between the two plates, after subtracting off the zero-field value (which is about 1% of the high-field value). The static yield stress was observed to have an accurate E^2 field strength dependence. The real and imaginary parts of the effective dielectric constants of the three samples were measured as a function of frequency, and are shown as symbols in Fig. 5. These data were used to determine the (frequency dependent) effective dielectric constants of the solid particles and the fluid, by assuming the water to *coat* the glass microspheres, with the excess water dispersed in silicone oil. Excellent fittings can be obtained, shown as the solid lines in Fig. 5.

With the material parameters thus determined, we compare the measured and predicted yield stress of the three samples in Fig. 6, again as a function of the applied electric field frequency. A reasonably good agreement is seen. Thus yield stress can be quantitatively predicted, provided the correct material parameters and geometric information are supplied.

This study shows that even a small amount of water can have a dramatic effect. And this is possible only if the water coats the solid particles, or inserts itself in the region of two touching microspheres. The thought that led to the discovery of the giant electrorheological effect, described below, is that if an OH group can somehow be fixed on the solid microspheres, then the dramatic effect seen here may be usefully utilized to enhance the ER effect, with no adverse consequences.

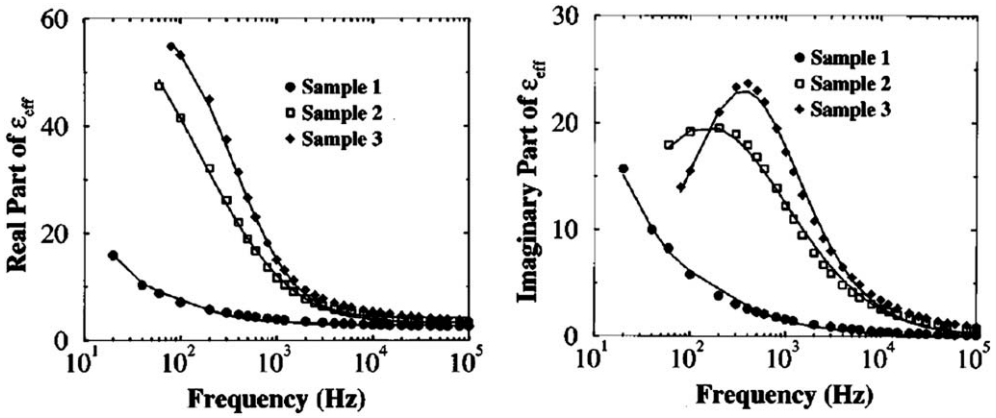

Fig. 5 The real and imaginary parts of the effective dielectric constants for the three samples plotted as a function of frequency. The symbols represent the experimental measurements and the lines are fitted theoretical calculations. The free material parameters are determined by the fittings.

3.3 Upper bounds

A particularly important result from the effective dielectric constant formulation is the upper bounds to the shear modulus and yield stress. This result can in fact be intuitively appreciated from eqn (10). Since both the shear modulus and yield stress are related to the real part of the effective dielectric constant, the upper bounds to these quantities will be determined by the divergence of $\bar{\varepsilon}_{zz}$. From eqn (10) this can only happen when the denominator on the right hand side vanishes. From the definition of s and the fact that s_u is always real and between 0 and 1, the divergence of $\bar{\varepsilon}_{zz}$ would happen when both s and s_u approach either 0 or 1. Here we explore only the case of the 0 limit. To obtain the physical upper bounds, we let $\varepsilon_s \to \infty$ so that $s \to 0$. We also note that s_u would approach zero only when the spheres touch. Hence we specify a (small) separation δ between the surfaces of the neighbouring spheres, and evaluate the shear modulus and yield stress as a function of the ratio δ/R, where R is the sphere radius. The upper bounds thus obtained are 1.9 (R/δ) for the shear modulus,[17,24] and $1.38\sqrt{R/\delta}$ for the static yield stress,[24] both in units of the energy density $\varepsilon_l E^2/8\pi$. For δ = 1 Å (atomic separation) and R = 20 μm, we get 15 120 $\varepsilon_l E^2$ for the maximum shear modulus and 617 $\varepsilon_l E^2$ for the maximum yield stress. If ε_l = 2.5 and E = 1 kV mm^{-1}, these expressions translate into 4 MPa and 8 kPa, respectively. It should be noted that both upper bounds increase monotonically with the size of the microspheres, and that the unit is quadratic in the electric field. Both are the consequences of the induced polarization mechanism. In particular, as the electrostatic energy density in a polarizable medium is generally given by $-\boldsymbol{P}\cdot\boldsymbol{E}$, where $\boldsymbol{P}$ is the dielectric polarization, then $\boldsymbol{P} \propto \boldsymbol{E}$ directly yields the quadratic dependence. The R dependence may be understood heuristically from the capacitance between two spheres, which diverges as $\ln(R/\delta)$.

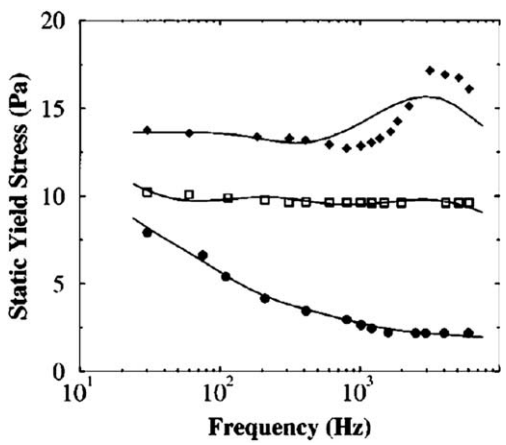

Fig. 6 The measured (symbols) and calculated (lines) static yield stress plotted as a function of frequency. From bottom to top: sample 1, sample 2, and sample 3, in order of increasing amounts of water.

To verify the particle size R and δ dependencies of the yield stress upper bound, doubly-coated microspheres were fabricated with a uniform-sized glassy core and nickel and titania (TiO_2) outer coatings, using sequentially electroless plating (for the nickel coating) and sol–gel (for the titania coating) methods.[18] Two different sizes of core glass microspheres, 1.5 μm and 50 μm in diameter, were used. A cross-sectional picture of the multiply-coated spheres is shown in Fig. 7(a–c).

Here the nickel coating serves the purpose of making the microspheres polarizable enough so that we can take s to be nearly zero, and the silica coating serves the purpose of setting a value for δ. In Fig. 8(a) and 8(b) we compare the measured yield stress values (symbols) with those calculated from the effective dielectric constant formulation. The increased size of the particles is clearly seen to increase the yield stress in approximately the square-root ratio as predicted by the upper bound expression. In addition, the absolute values of the measured yield stress are also well accounted for by the calculations using approximate values of the titania coating thicknesses. For comparison, we have also measured and calculated the yield stresses for pure glass spheres and those with just titania coatings. Both are orders of magnitude smaller (as seen by the lines lying close to the horizontal axis). The dashed line is the calculated value for pure titania spheres of similar size. It is also much smaller. The simple physical picture that emerges from these results is that (1) ER yield stress is closely related to the electrostatic energy of the system, and (2) for a given applied electric field, the electrostatic energy can be maximized by the field distribution and dielectric constant of the materials. The metallic coating of

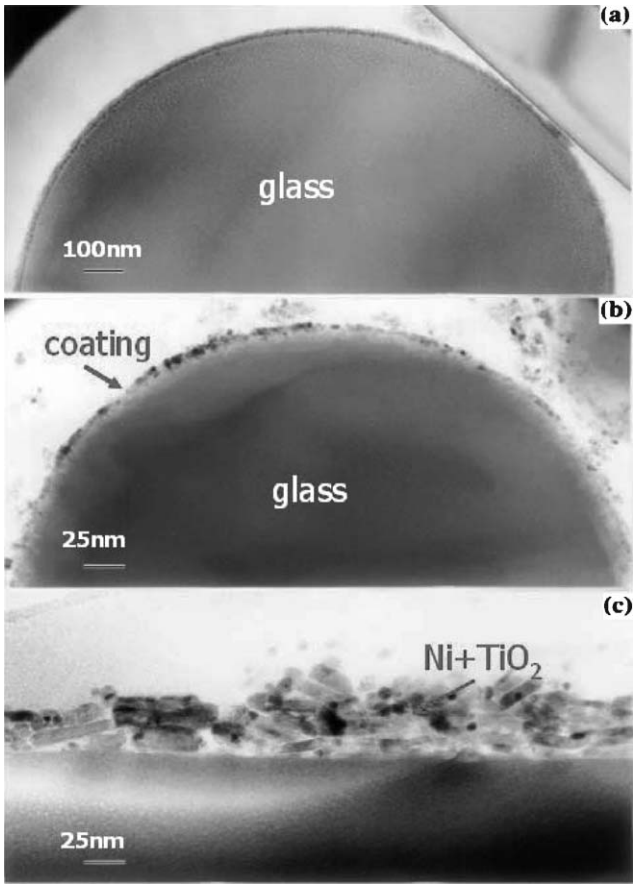

Fig. 7 Cross-sectional electron micrographs for (a) 1.5 μm nickel coated, (b) 1.5 μm doubly coated, and (c) 50 μm doubly coated particles. The scale bar is 100 nm, 25 nm and 25 nm for (a), (b), and (c), respectively. While in (a), the metal–glass interface is clearly visible, diffusion of Ni atoms, probably from the heating process, blurred this boundary, as shown in (b) and (c). The TiO_2 coating thickness is seen to be in the range of 10 to 30 nm for (b) and 25 to 60 nm for (c).

the doubly-coated microspheres limits the field distribution to the dielectric areas occupied by the titania coating and the silicone oil. The thin titania coatings ensure small separations, thus producing high internal fields. The enhanced ER effect is the result.

The doubly coated glassy microspheres are in a sense "ideal" for the ER effect, since solid metallic particles are too heavy and would quickly sediment. However, the requirement of large sphere size is not optimal from the applications point of view, since large microspheres also tend to sediment, unless the density can be matched with that of the fluid.

3.4 Anisotropy and nonlinearity of the effective dielectric constant

Since the theoretical approach is based on effective dielectric constant optimization, it is important to check experimentally if the dielectric constant indeed increases and displays anisotropy under the application of an electric field. However, measurement-wise it is difficult to determine the dielectric constant along the electric field direction, especially when the applied field is fairly large. In order to overcome this difficulty, we have utilized the similarity in the microstructure under an electric field with that under a magnetic field. For this experiment, special particles were prepared whereby silica spheres 35 $\pm$ 3 μm in diameter were coated with an inner Ni layer and an outer dielectric layer, such as lead zirconate titanate (PZT) or TiO_2, formed by using electroless plating and sol–gel processes, respectively. The microstructures formed by appling a magnetic field are shown in Fig. 9. The dielectric constants along the z (magnetic field direction) and x directions ($\bar{\varepsilon}_{zz}$ and $\bar{\varepsilon}_{xx}$), measured by an inductance, resistance and capacitance (LRC) meter, are shown in Fig. 10. It is seen that whereas the zz component of the effective dielectric constant displays an increasing trend with the magnetic field, just as expected, the xx component displays a slight decrease. And these trends are independent of whether the outer coating is PZT or TiO_2. The theory predictions of the asymptotic dielectric constant values, again obtained by using the spectral function approach,[21–24] are shown in Table 2. Here the inputs to the calculations are determined by the values of the real and imaginary parts of the effective dielectric constants when the system is isotropic (H = 0). It is seen that reasonably good agreement is

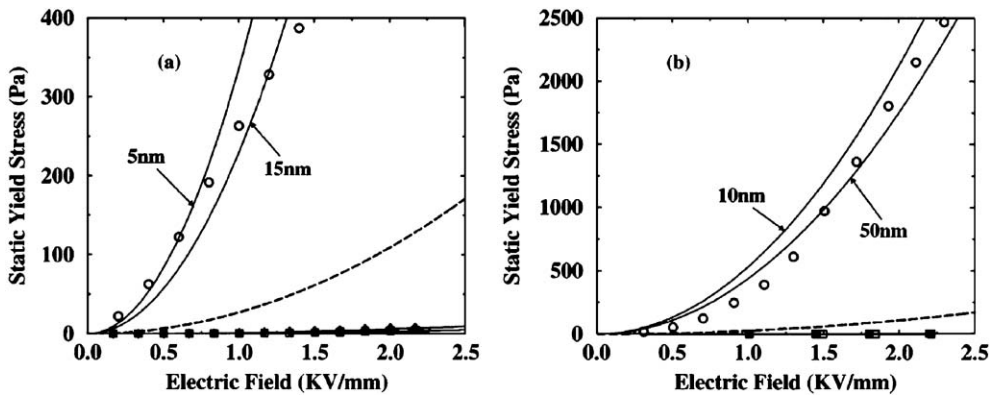

Fig. 8 The measured (symbols) and calculated (lines) static yield stress of an ER fluid using (a) 1.5 μm doubly coated particles, (b) 50 μm doubly coated particles. From the vertical scales it is seen that the larger particles exhibit a larger yield stress in roughly the square-root of the size ratio. For comparison, we have also shown the calculated yield stress for solid TiO_2 particles of the same sizes (dashed lines), as well as the measured yield stress for pure glass spheres (almost invisible as the open squares on the horizontal axis) of the same size, as well as the measured yield stress for glass spheres coated just by TiO_2, without the Ni (black diamonds on the horizontal axis) of the same size.

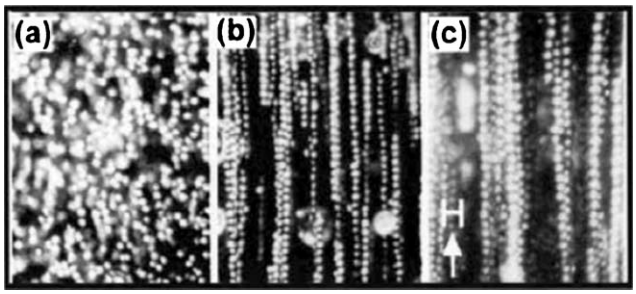

Fig. 9 Structure evolution as the magnetic field strength is increased. Here the field strengths for (a), (b) and (c) are 0, 30 and 200 G, respectively.

obtained. These theory–experiment comparisons thus provide strong support to the understanding of the ER mechanism as the result of induced polarization, made quantitatively predictable through the effective dielectric constant formulations with the Bergman–Milton spectral representation.

4. The giant electrorheological effect

In spite of the success in explaining the ER effect and the methods to optimize such effects, the upper bound of the yield stress implies that, for reasonably-sized particles and electric field values below the dielectric breakdown, the solid strength that can be practically achieved is still insufficient for most applications. However, these results also led to the search for a different type of ER fluid that relies on molecular dipoles rather than the induced polarization mechanism.

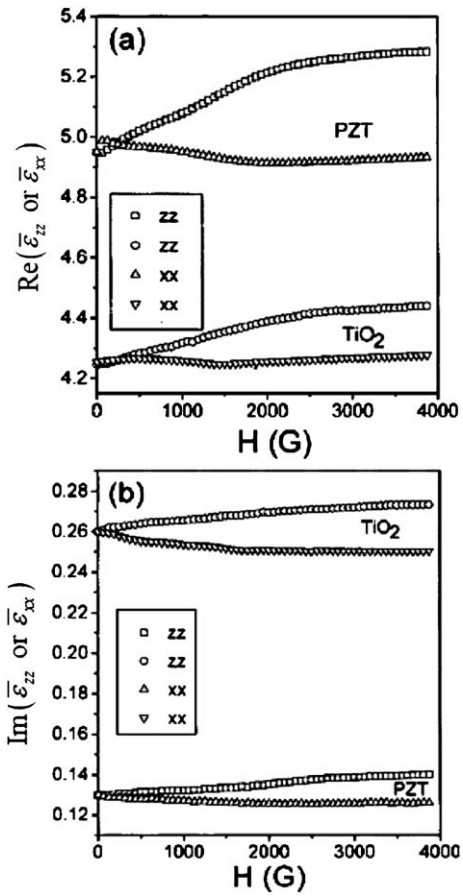

Fig. 10 Dependences of real (a) and imaginary (b) parts of the dielectric constant on applied magnetic field strength. Here the volume fraction is 0.27, and the frequency of the LCR meter is fixed at 1 kHz.

Table 2 Experimental and theoretical results of the real and imaginary parts of ER fluid dielectric constants measured along the z and x directions for the random and structured cases

		Theory		Experiment	
Structure		Re($\bar{\varepsilon}$)	Im($\bar{\varepsilon}$)	Re($\bar{\varepsilon}$)	Im($\bar{\varepsilon}$)
Random		Fitted	Fitted	4.95	0.13
PZT coating	*zz*	5.67	0.23	5.29	0.14
	xx	4.75	0.11	4.94	0.12
Random		Fitted	Fitted	4.26	0.26
TiO_2 coating	*zz*	4.56	0.37	4.44	0.28
	xx	4.15	0.23	4.25	0.25

There is a basic difference between the maximum (dimensionless) electric susceptibility of a collection of permanent dipoles and a system of polarizable particles, which may be heuristically quantified as follows. For a polarizable particle, the polarizability $\alpha = a^3\,(\varepsilon_s - 1)/(\varepsilon_s + 2)$ has a maximum value given by $\alpha = a^3$, attained by setting $\varepsilon_s \to \infty$ (here we exclude from our consideration negative ε_s values). If we take the largest possible number density of polarizable particles, $N = (4\pi a^3/3)^{-1}$, then the dimensionless $\chi = N\alpha$ has the maximum value of $3/4\pi = 0.239$. For a collection of molecular dipoles, the polarizability arises from the competition of thermal Brownian motion and the alignment effect of the applied electric field. The standard calculation leads to $\alpha = \mu_0{}^2/3k_BT$, where μ_0 denotes the molecular dipole moment, k_B the Boltzmann constant, and the T the temperature. If we let T be room temperature and μ_0 be one electronic charge separated from its opposite by 1 Å, then multiply that by N = (molecular volume)$^{-1}$, we obtain $\chi \approx 4$–50, depending on what we take for the molecular volume. The fact that there can be at least one order of magnitude difference in the maximum achievable values is easy to see. Of course, the molecular dipoles tend to form quadrupolar pairs, hence getting a dense collection of free molecular dipoles is not a simple matter. Yet the potential is there.

4.1 The giant electrorheological (GER) effect—particle structure and behavior

The study of the effect of water on the ER effect has prompted an attempt to fix OH groups on solid particles. While that was unsuccessful, it led to the discovery of urea-coated nanoparticles of barium titanate oxalate [$NH_2CONH_2{\cdot}BaTiO(C_2O_4)_2$] which, when dispersed in silicone oil, exhibits an ER effect orders of magnitude larger than those based on the induced polarization mechanism, exceeding the upper bound value by a large amount.[8,9] The GER effect also displays different electric field dependence to the yield stress, as well as the opposite dependence on the size of the particles. Thus the GER fluids represents a new paradigm.

In Fig. 11(a), a TEM picture shows that the structure of the GER particles consists of a ~50 nm core of barium titanate

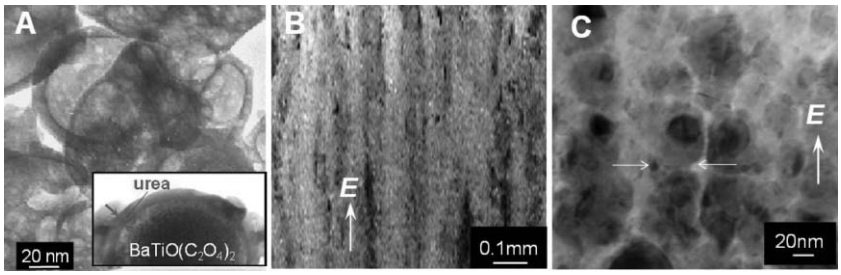

Fig. 11 Images of nanoparticles in GER suspensions. (a) TEM image of coated nanoparticles. Urea coatings are clearly seen. (b) Optical microscope image of a sample prepared in epoxy, solidified under an applied field E of 2 kV mm^{-1}. Columns aligned along the field direction are visible. (c) TEM image of a section of the column shown in (b). The arrows indicate one of the flattened interfaces.

oxalate, with a 5 nm coating of urea. In Fig. 11(b), an optical microscope picture shows column formation when an electric field was applied. In Fig. 11(c), a TEM picture shows that, under an electric field, the coatings of the nanoparticles are significantly deformed, indicating a degree of softness in the coating.

In Fig. 12, the measured yield stress and current density (shown in the inset) is plotted as a function of applied electric field. A prominent feature is the near-linear dependence of the yield stress on electric field. In accordance with the earlier discussion, this is only possible if the yield stress arises not from induced polarization, but rather from the saturation polarization of some permanent molecular dipoles, so that in the expression $-\boldsymbol{P}_0\cdot\boldsymbol{E}$ the polarization is a constant. The current density dependence on the electric field follows a so-called Poole–Frenkel mechanism, where the logarithm of the current density $\ln J \propto \sqrt{E}$ is a signature of charging carriers generated through activation barrier lowering by applied field, for ions held by the Coulomb potential of the counterions, *i.e.*, current density is due to the breakdown of the molecular dipoles.

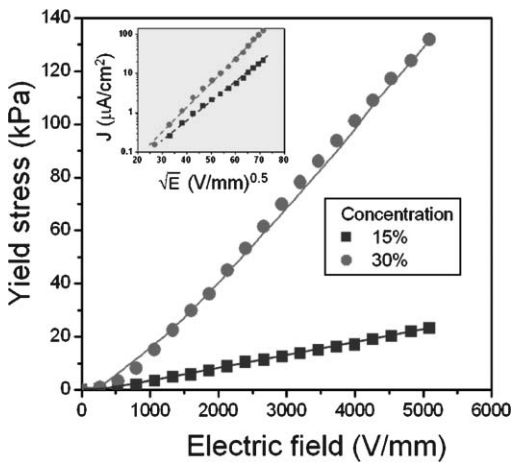

Fig. 12 Static yield stress plotted as a function of applied electric field for two solid concentrations. Symbols denote experiment; solid lines are theory. Inset: logarithm of the current density J plotted as a function of $\sqrt{E}$. The dashed straight lines serve to delineate the relationship $\ln J \propto \sqrt{E}$, indicating the mechanism of activation over the Coulomb barrier (the Poole–Frenkel effect). Note that at a very moderate field of 1000 V mm^{-1} the linear behavior of the yield stress is already established, indicating the existence of a saturated polarization layer.

4.2 A phenomenological model of the GER effect

The phenomenological GER model is based on the following elements: (1) the molecular dipoles of urea can form aligned dipolar layers in the *contact region* between two coated nanoparticles, under a moderate electric field of 1×10^6–10^7 V cm^{-1} [shown schematically in Fig. 13(a)]; (2) the equilibrium contact state is represented by the balance of the (attractive) electrostatic force with the (repulsive) elastic force; (3) the elastic deformation of two coated spheres in contact is given by the Hertzian solution;[36] (4) there is an electric field enhancement effect at the contact region, with an enhancement factor of $\sim 1 \times 10^2$ (estimated numerically by using the finite element method); (5) the shear stress is defined as the derivative of the total energy with respect to strain (which is just the shear distortion angle); and (6) the area of the contact region decreases under shear, and the yield stress is given by the stress value at the point of separation (zero contact area). This is illustrated schematically in Fig. 13(b). In the phenomenological model, there is only one adjustable parameter, given by the deformation modulus of the coating. It turns out that the value obtained from fitting is $\sim$0.1 GPa, similar to that for a liquid and agrees with the TEM observation that the coatings seem to be soft.

The predictions of the model are in good agreement with measured results, as seen from the solid lines in Fig. 12. In particular, the linear dependence on the applied electric field is a direct reflection of the surface saturation polarization. Another prediction of the model is that since the effect owes its origin to surface saturation polarization, more surface area (hence smaller particles) would enhance the GER effect. This turns out to be the case, opposite to the observed size scaling behavior of the induced polarization mechanism as described earlier.[9]

How does the surface saturation polarization come about? That is, what are the microscopic elements contributing to the statistical mechanics of the surface-aligned dipolar layers? While the end-to-end interaction between the dipoles is electrostatically favorable, side-to-side interaction between the dipoles is not. Hence to have two layers of aligned dipoles there must be some other contributing factors, such as the external electric field or chemical interactions, that also participate. A plausible hydrogen bonding model has been

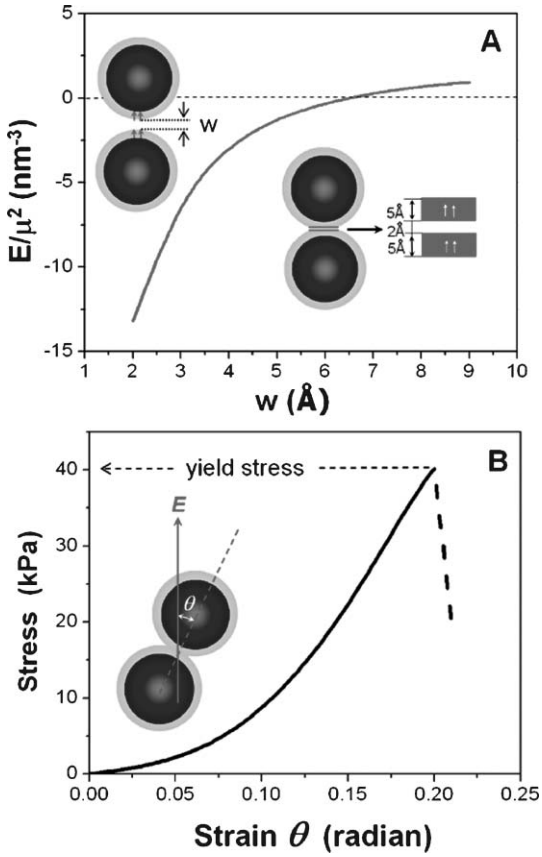

Fig. 13 Illustration of the phenomenological model with calculated results. (a) Upper left: schematic picture of our model, consisting of two coated spheres, each with a 50 nm diameter core and a 5 nm coating (both with $\varepsilon = 60$). The gap, with width w, has $\varepsilon = 2$ (for silicone oil). The solid curve shows the calculated interaction energy divided by μ^2 between two pairs of nearest-neighbour surface dipoles, each with $\mu = 4.6$ D and separated laterally by 4.5 Å ($\varepsilon = 1$ between the dipoles), when w increases from 2 Å. In (b), the stress numerically calculated from the finite element method, at an electric field of 2 kV mm^{-1}, is plotted as a function of the strain. The yield stress point corresponds to the point of separation between the two spheres.

proposed,[37] shown in Fig. 14. However, the energetics of the model, as well as other statistical considerations, are topics still to be further investigated.

5. Concluding remarks

Research into electrorheological fluids is at a stage where both basic and applied aspects present open challenges. In the basic scientific aspect, both the microscopic GER mechanism, and the dynamics of the ER effect, *e.g.*, under high shear rates, are to be further explored. In applied aspects, the potential of active mechanical devices, from active dampers to ER clutches and brakes, as well as many others, remain to be commercially realized. It is thus an exciting prospect to contemplate the future in which ER fluid research can provide an inroad to our understanding of molecular-scale response to moderate external electric fields, as well as the many active mechanical devices which can fully utilize the potential of the material property inherent to ER fluids—the rapid and

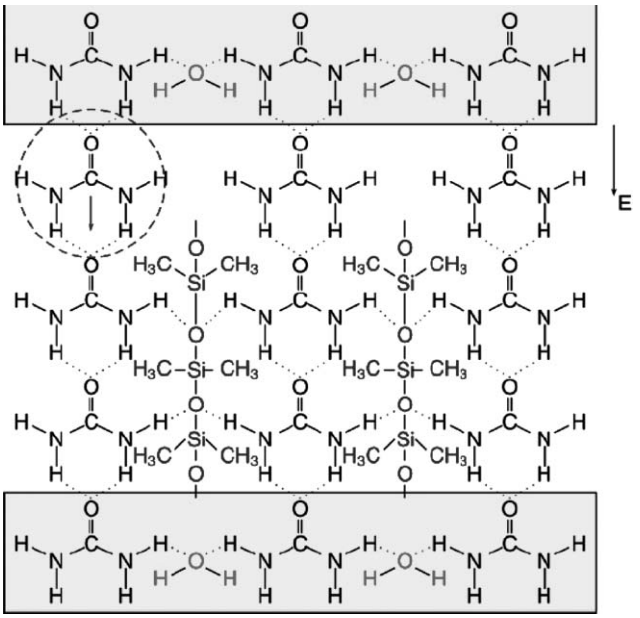

Fig. 14 A schematic hydrogen bonding (indicated by the dotted lines) network favoring the formation of parallel alignment of urea molecular dipoles. The urea molecular dipole unit is indicated by the dashed line, with direction as shown.

reversible fluid–solid transformation, controllable through an electric field.

References

1 *Electrorheological Fluids, Magnetorheological Suspensions and Associated Technology, Proceedings of the 5th International Conference*, ed. W. A. Bullough, World Scientific, Singapore, 1996.
2 J. D. Carlson, P. Sheng and W. Wen, in *Actuator 2006 – Proceedings of the 10th International Conference on New Actuators*, ed. H. Borgmann, HVG Hanseatische Veranstaltungs-GmbH, Bremen, 2006, pp. 235–240.
3 *Electrorheological Fluids, Magnetorheological Suspensions and Their Applications, Proceedings of the 6th International Conference*, ed. M. Nakano and K. Koyama, World Scientific, Singapore, 1999.
4 *Electrorheological Fluids, Magnetorheological Suspensions and Their Applications, Proceedings of the 7th International Conference*, ed. R. Tao, World Scientific, Singapore, 2000.
5 *Electrorheological Fluids and Magnetorheological Suspensions, Proceedings of the 8th International Conference*, ed. G. Bossis, World Scientific, Singapore, 2002.
6 *Electrorheological Fluids and Magnetorheological Suspensions, Proceedings of the 9th International Conference*, ed. Q. Lu, R. Shen and J. Liu, World Scientific, Singapore, 2005.
7 J. D. Carlson, R. Stanway and A. R. Johnson, presented in part at the Actuator 2004, 9th International Conference on New Actuators, Bremen, Germany, 2004.
8 W. Wen, X. Huang, S. Yang, K. Lu and P. Sheng, *Nat. Mater.*, 2003, **2**, 727.
9 W. Wen, X. Huang and P. Sheng, *Appl. Phys. Lett.*, 2004, **85**, 299.
10 W. M. Winslow, *J. Appl. Phys.*, 1949, **20**, 1137.
11 *Electrorheological Fluids: Mechanisms, Properties, Technology and Applications*, ed. R. Tao and G. D. Roy, World Scientific, Singapore, 1994.
12 R. Tao and J. M. Sun, *Phys. Rev. Lett.*, 1991, **67**, 398.
13 D. G. Klingenberg, F. V. Swol and C. F. Zukoski, *J. Chem. Phys.*, 1989, **91**, 7888.
14 K. C. Hass, *Phys. Rev. E*, 1993, **47**, 3362.
15 L. C. Davis, *Appl. Phys. Lett.*, 1992, **60**, 319.
16 L. C. Davis, *J. Appl. Phys.*, 1992, **72**, 1334.

17 H. R. Ma, W. J. Wen, W. Y. Tam and P. Sheng, *Phys. Rev. Lett.*, 1996, **77**, 2499.
18 W. Y. Tam, G. H. Yi, W. J. Wen, H. R. Ma, M. M. T. Loy and P. Sheng, *Phys. Rev. Lett.*, 1997, **78**, 2987.
19 T. J. Chen, R. N. Zitter and R. Tao, *Phys. Rev. Lett.*, 1992, **68**, 2555.
20 Y. Chen, A. E. Sprecher and H. Conrad, *J. Appl. Phys.*, 1991, **70**, 6796.
21 *Solid State Physics*, ed. D. J. Bergman and D. Stroud, Academic Press, 1992, vol. 46.
22 G. W. Milton, *Appl. Phys. A*, 1981, **26**, 1207.
23 G. W. Milton, *J. Appl. Phys.*, 1980, **52**, 5286.
24 H. Ma, W. Wen, W. Y. Tam and P. Sheng, *Adv. Phys.*, 2003, **52**, 343.
25 R. Tao and Q. Jiang, *Phys. Rev. Lett.*, 1994, **73**, 205.
26 Y. Chen and H. Conrad, *Int. J. Mod. Phys. B*, 1994, **8**, 2895.
27 H. Conrad and A. F. Sprecher, *J. Stat. Phys.*, 1994, **64**, 1073.
28 Z. W. Wang, H. P. Fang, Z. F. Lin and L. W. Zhou, *Phys. Rev. E*, 2000, **61**, 6837.
29 D. J. Klingenberg, F. V. Swol and C. F. Zukoski, *J. Chem. Phys.*, 1991, **94**, 6160.
30 X. Tang, C. Wu and H. Conrad, *J. Appl. Phys.*, 1995, **78**, 4183.
31 W. J. Wen, N. Wang, H. R. Ma, Z. F. Lin, W. Y. Tam, C. T. Chan and P. Sheng, *Phys. Rev. Lett.*, 1999, **82**, 4248.
32 T. Hao, A. Kawai and F. Ikazaki, *Langmuir*, 1999, **16**, 3058.
33 X. D. Duan, W. L. Luo and W. Wu, *J. Phys. D*, 2000, **33**, 3102.
34 H. J. Choi, M. S. Cho, J. W. Kim, C. A. Kim and M. S. John, *Appl. Phys. Lett.*, 2001, **78**, 3806.
35 W. J. Wen, H. R. Ma, W. Y. Tam and P. Sheng, *Phys. Rev. E*, 1997, **55**, R1294.
36 *Theory of Elasticity*, ed. L. D. Landau and E. M. Lifshitz, Addison-Wesley, Reading, Massachusettts, 2nd edn, 1969.
37 X. Huang, W. Wen, S. Yang and P. Sheng, *Solid State Commun.*, 2006, **139**, 581.

